Cancer Management and Research

Elevate Series

Open Access Full Text Article

ORIGINAL RESEARCH

Blood Stasis Constitution Ointment Exerts Anti-Lung Cancer Effects: A Study Integrating Network Pharmacology, Transcriptomics, and Experimental Validation

Qiaozhi Wang[1], Juhe Wang[2], Chuanhao Dai[1], Tianming Lu[1], Xingjiang Xiong[2], Shuo Shen[1], Qiuyan Guo[1], Hu You[2], Maobo Du[1]

[1]Institute of Chinese Materia Medica, China Academy of Chinese Medical Sciences, Beijing, 100700, People's Republic of China; [2]Gu Zheng Bao He Internet Hospital, Chengdu, Sichuan Province, 610000, People's Republic of China

Correspondence: Maobo Du, Institute of Chinese Materia Medica, China Academy of Chinese Medical Sciences, Beijing, 100700, People's Republic of China, Email mbdu@icmm.ac.cn; Hu You, Gu Zheng Bao He Internet Hospital, Chengdu, Sichuan Province, 610000, People's Republic of China, Email 364577807@qq.com

Aim of the Study: To analyze the chemical components of BSCO, evaluate its effects on lung cancer through vivo and vitro experiments, reveal its underlying mechanism in a rat model of LC.

Methods: Ultra-high performance liquid chromatography with quadrupole time-of-flight mass spectrometry was used to identify components of BSCO. A Lewis lung cancer model was established in mice to evaluate the effects of BSCO by observing tissue morphology, whole animal imaging, and determination of serum biochemical indicators. The effects of BSCO on Lewis cancer cells in vitro were assessed using a CCK-8 cell proliferation assay. Network pharmacology and transcriptomics analysis was used to predict their targets and signaling pathways associated with lung cancer. The mRNA expressions of target genes were measured by RT-qPCR.

Results: Twenty major chemical components of BSCO were identified. BSCO effectively inhibited tumor growth in the Lewis lung cancer mouse model and normalized serum markers of cancer to varying degrees. The IC_{50} of BSCO on Lewis cell proliferation was 173 mg/mL. Low- and high-dose BSCO-containing drug serum inhibited proliferation of Lewis cells after 24 and 48 h incubation. Integrated network pharmacology and transcriptomic analyses suggest that BSCO may exert anti-tumor effects through the PI3K-Akt signaling pathway, with TP53, IL6, CDKN1A, and KIT identified as potential key targets within this pathway. The reliability of the transcriptomic results was confirmed by verifying some lung cancer-related genes through RT-qPCR. BSCO was evaluated against model control and cyclophosphamide. A key follow-up step will be to perform protein-level validation, which confirms the observed transcriptomic signals.

Conclusion: BSCO significantly inhibited lung cancer growth in vitro and in vivo. Network pharmacology and transcriptomics suggested that its anti-cancer effects might involve the PI3K-Akt signaling pathway, TP53, IL6, CDKN1A, and KIT may be its key targets.

Keywords: blood stasis constitution ointment, BSCO, UPLC-Q-TOF-MS, network pharmacology, lung cancer, transcriptomics analysis, medicine-food homologous substances

Introduction

Lung cancer is still the leading cause of cancer deaths worldwide and the number of cases continues to rise in most countries.[1] It is characterized by a high mortality rate after diagnosis and it has been estimated by the International Agency for Research on Cancer (IARC) under the World Health Organization (WHO) that there were about 2.2 million new cases and 1.8 million deaths in 2020.[2,3]

The pathogenesis of lung cancer is still unclear in modern medicine. Recently, it has been linked to the lung microbiome, and smoking is the main risk factor.[4,5] According to the theory of traditional Chinese medicine (TCM), lung cancer belongs to the category of "lung accumulation", and the main pathogenesis is "depression". It is primarily

Received: 27 August 2025
Accepted: 9 December 2025
Published: 17 December 2025

due to deficiency of lung qi, which leads to internal obstruction of phlegm and turbidity in the body, followed by invasion of the lungs by external pathogens. Ultimately, this leads to qi stagnation and dampness obstruction, internal stagnation of phlegm and turbidity, phlegm and blood stasis interconnections, and the pathogenesis of transforming toxins into cancers.[6]

Clinical treatment of lung cancer domestically and internationally includes surgery, radiotherapy, chemotherapy, ablation, targeted therapy, and immunotherapy.[7] Currently, surgical treatment remains the first choice, while the survival rate of targeted therapy drugs is not high.[8,9] New, effective drugs are required to improve clinical survival. Using TCM for 180 days or more was linked to a 59% lower risk of disease progression compared to not using TCM.[10] Kangai, Kanglaite, Aidi, and Compound Kushen injections all demonstrated significant efficacy and safety advantages. Notably, Aidi combined with GP (gemcitabine + cisplatin) achieved the highest objective response rate (ORR) of 79.0%.[11]

The Chinese medicine constitution is a comprehensive and relatively stable inherent trait that is based on innate and acquired characteristics of the human body during life processes.[12] The Chinese medicine constitution has been widely recognized internationally.[13] According to TCM theory, one of the core elements of lung cancer is an unbalanced constitution, with blood stasis being the representative constitution.[14] Blood stasis can lead to a hypercoagulable state, which not only increases the risk of thrombosis in lung cancer patients, but also contributes to tumor proliferation, severely affecting quality of life and prognosis in these patients.[15]

Oral Paste, also known as "nourishing ointment," is a Chinese medicinal paste used for health preservation. These pastes are effective in improving the constitution and offering lasting therapeutic effects.[16] Medicine-food homologous substances refer to those substances that are traditionally used as food and included in the "Pharmacopoeia of the People's Republic of China". The constitution, dietary therapy, and oral pastes are closely related.

Building on these principles, they have carefully formulated blood stasis constitution ointment (BSCO) based on the fundamental prescription meanings and concepts of two classic renowned formulas, namely "Xuefu Zhuyu Decoction" and "Buyang Huanwu Decoction" appearing in Yilin Gaicuo by Wang Qingren in 1830.

Xuefu Zhuyu and Buyang Huanwu decoctions are well-known TCM prescriptions that are used to treat blood stasis syndrome. They are currently employed extensively in the management of blood stasis-related diseases, and substantial therapeutic efficacy has been demonstrated.[17,18] Recent studies have shown the palliative effect of Xuefu Zhuyu and Buyang Huanwu decoctions on symptoms associated with lung cancer.[19,20] Higher overall clinical efficacy was observed in patients receiving Xuefu Zhuyu decoction in conjunction with standard treatment, compared with those receiving standard treatment alone.

The formulation addresses four aspects: Reinforce healthy qi, correcting imbalances, eliminate pathogenic factors, and flavoring. Huangdi Neijing suggests that "When the healthy qi is strong within, pathogenic factors cannot act".[21] This formula is made up of 16 traditional Chinese ingredients, including *Panax ginseng* C.A.Mey, oxhide gelatin, E'Jiao (Colla corii asini), *Tremella fuciformis* Berk, *Lycium chinense* Mill, *Nelumbo nucifera* Gaertn, *Prunus persica* (L). Batsch, *Pueraria alopecuroides* Craib, *Rosae rugosae* Thunb. *Hordeum vulgare* L, *Poria cocos (*Schw). Wolf, *Citrus reticulata* Blanco, *Crataegus pinnatifida* Bunge and *Hippophae rhamnoides* L, *Vigna umbellata* (Thunb). Ohwi & H.Ohashi and *Allium macrostemon* Bunge. Modern evidence supports the roles of several key ingredients: *Panax ginseng* shows immunomodulatory and homeostasis-supporting effects.[22] E'Jiao exhibits hematinic and blood-nourishing actions.[23] *Lycium chinense* and *Tremella fuciformis* polysaccharides provide nutritive and immunomodulatory support,[24,25] *Crataegus pinnatifida* contributes to digestion and lipid regulation.[26] Oligosaccharide maltose is used to provide shape and texture and improve the flavor without the concern of raising blood sugar levels, making it more acceptable to the public.[27]

UPLC-Q-TOF-MS is widely used to identify the active compounds of traditional herbal decoctions by enabling high-resolution, accurate-mass profiling and rapid MS/MS-based analysis across complex matrices, allowing deconvolution of co-eluting constituents, assignment of elemental formulas, and structure annotation from rich fragment ions.[28,29]

In summary, although BSCO has extensive support from traditional Chinese medicine theories, the therapeutic efficacy of BSCO in treating lung cancer (LC) and its potential molecular mechanisms remain unclear. This research is based on the doctrine of constitution and medicinal paste, drawing on classic prescriptions and utilizing medicine food homology substances that meet safety requirements to create BSCO. This study utilized ultra-high performance liquid

chromatography with quadrupole time-of-flight mass spectrometry (UPLC-Q-TOF-MS) to identify the active components of BSCO. In vitro and in vivo experiments were conducted to evaluate the effect of BSCO on lung cancer. Additionally, network pharmacology and transcriptomics were integrated to predict its target points, providing evidence-based support for its efficacy.

Materials and Methods

Reagents and Instruments

Blood stasis constitution ointment was obtained from Sichuan Guzheng Baohe Health Management Co., Ltd., chromatographic grade methanol was purchased from Fisher Scientific, and pure water was from Hangzhou Wahaha Group Co., Ltd.

Instruments: ACQUITY UPLC H-Class ultra-high performance liquid chromatography system and Vion IMS Q-TOF high-resolution mass spectrometer (Waters Corporation, USA); ME155DU electronic balance (Mettler-Toledo Instruments); BioTek Synergy H1 Multifunctional Microplate Detector (Agilent); QX200™ Droplet Digital™ PCR System (Bio-RAD).

UPLC-Q-TOF-MS Analysis

UPLC-Q-TOF-MS Conditions

An ACQUITY UPLC BEH C18 column (2.1 × 50 mm, 1.7 μm) was used, with a mobile phase consisting of 0.1% aqueous formic acid solution (A) and methanol (B) and gradient elution (0–15 min, 25–65% B; 15–19 min, 65–80% B; 19–20 min, 80–25% B). The flow rate was set at 0.3 mL/min, and the column temperature was maintained at 35 °C. Electrospray ionization (ESI) was used in positive ion mode scanning. The desolvation N_2 gas flow rate was set at 1000 L/h, with a desolvation gas temperature of 450 °C. The cone gas flow rate was 50 L/h, the capillary voltage was 3.0 kV, the cone voltage was 30 V, and the ion source temperature was 120 °C.

Preparation of Test Solution

A 0.2 g of BSCO was weighed and placed in a 100 mL stoppered conical flask. Then, 30% methanol (50 mL) was added and the weight recorded. The test sample was subjected to 30 min of ultrasonic extraction at 300 W. After cooling, the weight was made up with 30% methanol and the solution was mixed thoroughly. The solution sample was passed through a 0.22 μm microporous filter membrane, and the resulting filtrate was gathered for analysis.

Animal Experiments

Animals

All animal procedures were approved by the Animal Ethics Committee of the Institute of Chinese Materia Medica, China Academy of Chinese Medical Sciences (Approval No.202313195 and No.202313259) and were conducted in accordance with the Guide for the Care and Use of Laboratory Animals; reporting follows ARRIVE 2.0 guidelines.

Male specific pathogen-free (SPF) Sprague Dawley (SD) rats (180–200 g) and male SPF C57BL/6J mice (18–22 g) were purchased from Beijing Vital River Laboratory Animal Technology Co., Ltd. (Beijing, China), permit number: SCXK (Jing) 2021–0011.

Assessment of Lewis Cell Growth in Mice

The Lewis lung cancer mouse model was used to evaluate the therapeutic effect of BSCO on lung cancer, observing tissue morphology, in vivo imaging of the mice, and determination of multiple serum biochemical indicators.[30]

Experimental Animals, Grouping, and Model Construction

Seventy-two C57BL/6 male mice weighing 20 ± 2 g were used for the experiments. The animals were housed at room temperature (25 ± 1 °C), relative humidity of 60%, and normal alternation of day and night for 12 h, with free access to food and water. After acclimatization, the animals were randomly divided into six groups of 12 animals using a computer-generated sequence: blank control, model, positive drug cyclophosphamide (Cytoxan, 0.2 mL/10 g), and BSCO low, medium, and high dose (0.2, 0.4, and 0.8 mL/10 g) groups. Animal doses were translated from the intended

human dose using body-surface-area (BSA) allometric scaling with FDA-recommended Km factors. The high-dose group is derived from the conversion of the clinical human administration dose.

The mice were anesthetized and placed on the operating table in the right lateral position. The left armpit was shaved and disinfected with 75% ethanol. A 5 mm incision was made in the left axilla at the upper edge of the rib arch at the anterior line at about 1.5 cm. The skin and subcutaneous tissues were separated, and the chest wall was exposed until the pink lobes of the lungs could be seen moving due to respiration. Serum-free medium or phosphate buffered saline (50 μL) containing tumor cells (10^6 cells per mouse) was mixed with Matrigel matrix (50 μL) on ice and injected vertically into the left lung with a micro feeder at a depth of about 3 mm. After 20 s the needle was removed and the incision closed with 1 or 2 stitches. The cell line was mouse-derived LLC (Lewis)-luc cells (luciferase-labeled mouse lung cancer cells, No. LZQ0009, Shanghai Zhongqiao Xinzhou Company) cultured in Dulbecco's Modified Eagle Medium containing 10% fetal bovine serum (FBS). After successful establishment of the model, the low, medium, and high dose BSCO groups were dosed by oral gavage once a day (0.2, 0.4, or 0.8 mL/10 g). The positive drug group was dosed by intraperitoneal injection with cyclophosphamide (0.2 mL/10 g) every other day. The model group received an equivalent volume of distilled water, and dosing continued for 14 days.

Histomorphology Observation

Histomorphological assessments were conducted following established procedures.[31] Outcome assessments (including H&E histopathology) were performed by investigators/pathologists blinded to group allocation. After the mice had been euthanized, lung tissue (1 lobe) was taken and fixed in formaldehyde, embedded in paraffin, and stained with hematoxylin and eosin (H&E). Morphological changes were observed by light microscopy (n = 3 in each group). The remaining lung tissues were frozen and stored.

Determination of Serum Biochemical Indexes

Blood samples were obtained 24 h after the final administration by removing the eyeballs. After resting at 4 °C for 30 min, the samples were centrifuged at 3500 r/min for 10 min and the supernatants stored at −80 °C for analysis. The serum biochemical indexes determined in this study included: superoxide dismutase (SOD), glutathione peroxidase (GSH-Px), catalase (CAT), hexokinase 2 (HK2), phosphofructokinase (PFK), malondialdehyde (MDA), glucose transporter protein 1 (GLUT1) and pyruvate kinase (PK).

Cell Culture and Evaluation of Lung Cancer Cell Growth

Cell culture and growth assays were performed as previously described, with minor modifications.[32] Lewis cells were grown in RPMI medium with 10% FBS at 37 °C in a humidified atmosphere with 5% CO2. When cell growth reached 70% to 80%, they were digested with trypsin and passaged. Tumor cells in the logarithmic growth phase were incubated in 96-well plates for 12 h. After the cells had attached to the wall, they were treated with different concentrations of BSCO for 24, 48, and 72 h. The negative control group was Lewis cells cultured in culture medium. Cell viability was determined using the CCK-8 method.

Serum Pharmacology

With reference to the reported method for serum pharmacology of traditional Chinese medicine,[33] rats were randomly divided into blank control (n = 15), high-dose (n = 5), low-dose (n = 5), and cyclophosphamide control (n = 5) groups, the dosage used was consistent with that in the previous experiment. The blank control group received an equal volume of saline by oral gavage for 7 d. Blood was collected under sterile conditions 1 h after the last gavage, and the serum was separated and filtered to remove bacteria. Lewis cells in the logarithmic growth phase were divided into five groups: normal control (10% normal culture serum + RPMI-1640 medium); blank serum (10% blank serum + RPMI-1640 medium); positive control group (10% cyclophosphamide group serum + RPMI-1640 medium); BSCO low-dose group (10% low-dose group serum + RPMI-1640 medium); BSCO high-dose group (10% high-dose group serum + RPMI-1640 medium). After culture for 24, 48 or 72 h, cell proliferation was analyzed using the CCK-8 method.

Network Pharmacology Analysis

BSCO Active Ingredients and Target Screening

After identification of all active chemical components by UPLC-Q-TOF-MS, their structural data were uploaded to the SwissADME platform (http://www.swissadme.ch). Chemical components meeting at least two of Lipinski's Rule of Five (RO5) criteria were included in the active compounds, together with compounds for which in vivo activity studies had been reported in the literature. Other compounds were excluded. Chemical structures were obtained from the PubChem database (https://pubchem.ncbi.nlm.nih.gov/). Potential targets of BSCO components were obtained from three databases: TCMSP (https://old.tcmsp-e.com/tcmsp.php/), ETCM2.0 (http://www.tcmip.cn/ETCM2/front/) and Swiss Target Prediction (http://www.swisstargetprediction.ch/). The targets obtained from the three databases were combined and duplicates removed to obtain the therapeutic targets of BSCO. The names of all targets were cross-checked using the UniProt online protein database (https://www.uniprot.org/).

Identification of Lung Cancer Specific Targets

Relevant targets were searched for using the keywords "lung cancer" and "lung cancer tumor" in four databases: Therapeutic Target Database (TTD, https://db.idrblab.net/ttd/), GeneCards (https://www.genecards.org/), Online Mendelian Inheritance in Man (OMIM, https://omim.org/) and DisGeNET (https://www.disgenet.org/). The targets obtained were combined and duplicates removed to obtain therapeutic targets for lung cancer. The names of all targets were cross-checked using the UniProt online protein database (https://www.uniprot.org/).

Hub Gene PPI Network and Pathway Enrichment Analysis

The Venn online analysis platform (http://jvenn.toulouse.ina.fr/app/example.html) was used to draw a Venn diagram of the overlapping targets between drugs and diseases. The data were then input into the STRING database (https://string-db.org/) to construct a protein-protein interaction (PPI) network. Cytoscape 3.10.2 was used to visualize the BSCO-lung cancer targets PPI network. Network analyzers are used to calculate topological parameters in the network. The median node degree (Degree), median betweenness centrality (BC), and median closeness centrality (CC), each calculated twice, were used as evaluation criteria for the nodes. The obtained targets were imported into Cytoscape 3.10.2, and the hub gene PPI network was constructed.

In parallel, GO and KEGG pathway enrichment analyses were conducted using the Metascape database (http://metascape.org/gp/index.html). Pathways with $P \leq 0.01$ were selected.

Transcriptomics Sequencing

Total RNA was isolated from murine tumor tissues with TRIzol® Reagent (Invitrogen), followed by DNase I (TaKaRa) treatment to eliminate genomic DNA. RNA integrity and concentration were evaluated using a 2100 Bioanalyzer and NanoDrop ND-2000 spectrophotometer, respectively. Sequencing libraries were prepared with the TruSeq™ RNA Sample Preparation Kit (Illumina) through polyA selection, RNA fragmentation, cDNA synthesis, and 15-cycle PCR amplification. Paired-end sequencing (150 bp × 2) was conducted on the Illumina NovaSeq 6000 platform. Raw reads underwent adapter trimming and quality control via Trimmomatic, then aligned to the reference genome using hisat2. Alignment quality was assessed by qualimap_v2.2.1, and gene-level read counts generated by htseq. Differentially expressed genes (DEGs) were identified with edgeR ($|\log_2 FC| > 1.5$, FDR < 0.05). Functional enrichment analysis for KEGG pathways, with significant enrichment determined by Bonferroni-corrected P-value < 0.05.

Quantitative Real-Time PCR (q-PCR)

Genomic DNA removal was performed in triplicate using TaKaRa RR047A (10 μL reaction volume per replicate). Subsequently, reverse transcription reactions were set up in triplicate (20 μL each). Target gene amplification was carried out by PCR, using primers listed in Table 1 (triplicate 20 μL reactions). PCR products were separated on 2% agarose gels, purified using the AxyPrep DNA Gel Extraction Kit (Axygen Biosciences, Union City, CA, US) as per the manufacturer's protocol, and quantified with QuantiFluor™-ST (Promega, U.S). Quantitative real-time PCR (qPCR)

Table 1 Primers for Quantitative PCR

Gene	Forward Primer (5′-3′)	Reverse Primer (5′-3′)
CDKN1A	ACCAGCCTGACAGGTAAGGA	TGCTGAGCCATCTCTTCAGC
KIT	GCCAGGAGACGCTGACTATC	GTGTTCTGCTGCCAAGAAGC
VEGFA	GTCAGCAGGAGAAGGTCACC	TGGACGGCGTCAATTCTGAA
JUP	TACCAGATGTCCACAACGGC	TCATCGTTGAGCAGCTTGGT
DLL1	ACTCTCTCGGTTCCTAGCGT	CACAGAGCAACCTTCTCCGT
KLF4	AGTGCCAGAAGTGTGACAGG	CCATGATTGTAGCGCTTGCC
S100A8	GCAGGTGAGGAGGTGCTATG	TCACCATCGCAAGGAACTCC
S100A9	TTGCCTAACAGTGGCCAGAG	CTCTCACAAGCCAAGCCTCA
HSPA5	GCGTCGGTGTGTTCAAGAAC	TCATTCCAAGTGCGTCCGAT
VIM	CCACCTTCGAAGCCATGTCT	GTCCACCGAGTCTTGAAGCA
GAPDH	GGTTGTCTCCTGCGACTTCA	TGGTCCAGGGTTTCTTACTCC

detection was performed in triplicate (20 μL reactions). Relative mRNA expression levels within each sample were normalized to GAPDH and calculated using the $2^{-\Delta\Delta CT}$ method.

Statistical Analysis

Data were analyzed using GraphPad Prism 5.0 software and expressed as mean ± standard deviation. Comparisons between groups were performed by one-way ANOVA. * $P < 0.05$, ** $P < 0.01$, *** $P < 0.001$, **** $P < 0.0001$; ns indicates no significant difference.

Results

Identification of the Main Chemical Components of BSCO by UPLC-Q-TOF-MS

The base peak chromatogram of BSCO is shown in Figure 1 (Base peak chromatogram of BSCO in positive ion mode). Using the accurate relative molecular mass data, information on secondary fragment ions, and literature data, a total of 20 chemical components were identified, as detailed in Table 2.

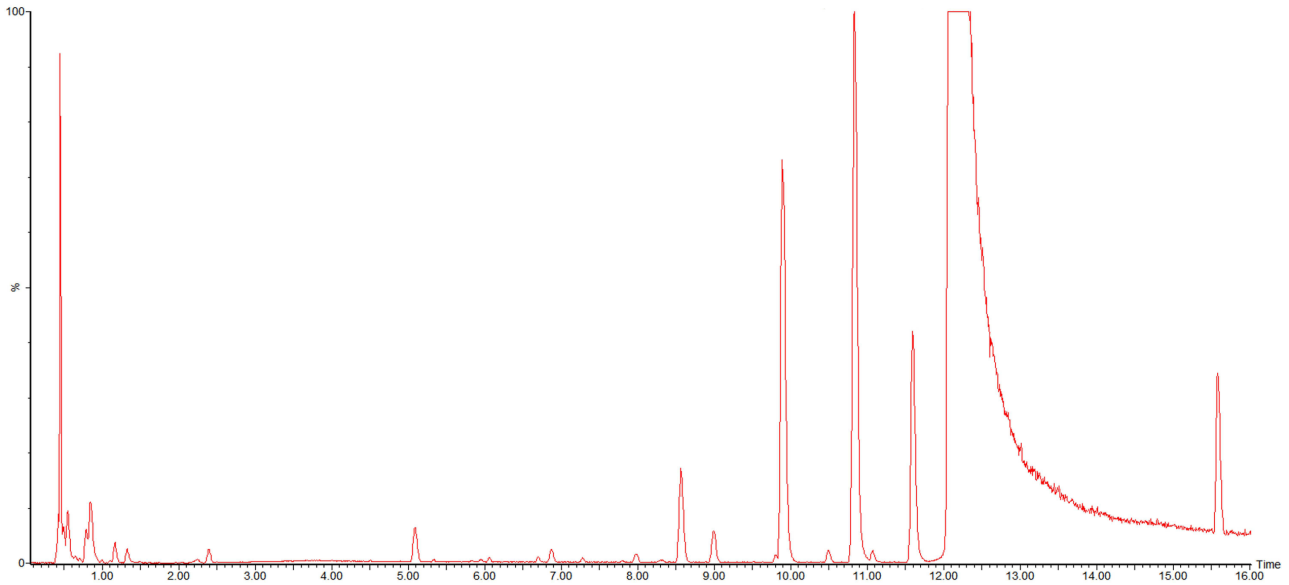

Figure 1 Base peak chromatogram of BSCO in positive ion mode.

Table 2 Main Chemical Components of BSCO

No.	Compounds	Formula	Chemical Structure	Ion Mode	Found Mass	Theo. MASS	Error/×10^{-6}
1	L-tyrosine	$C_9H_{11}NO_3$	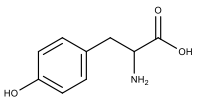	$[M+Na]^+$	204.0602	204.0637	−17.15
2	Purine	$C_5H_4N_4$	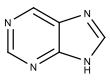	$[M+H]^+$	136.0663	136.0623	29.40
3	Adenosine	$C_{10}H_{13}N_5O_4$	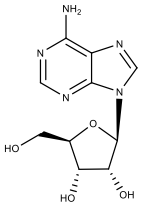	$[M+H]^+$	268.1082	268.1046	13.43
4	Caffeic acid phenethyl ester	$C_{17}H_{16}O_4$	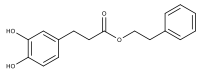	$[M+NH_4]^+$	302.1380	302.1392	−3.97
5	Limonin	$C_{26}H_{30}O_8$	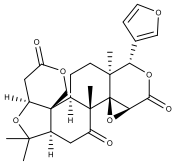	$[M+H]^+$	471.2026	471.2019	1.49
6	Naringin	$C_{27}H_{32}O_{14}$	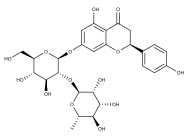	$[M+H]^+$	581.1862	581.1870	−1.38
7	Nobiletin	$C_{21}H_{23}O_8$	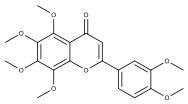	$[M+H]^+$	403.1416	403.1393	5.71
8	Daidzin	$C_{21}H_{20}O_9$	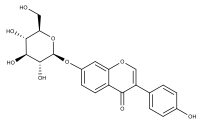	$[M+H]^+$	417.1206	417.1186	4.79

(*Continued*)

https://doi.org/10.2147/CMAR.S563551

Table 2 (Continued).

No.	Compounds	Formula	Chemical Structure	Ion Mode	Found Mass	Theo. MASS	Error/×10^{-6}
9	Delta-Carotene	$C_{40}H_{56}$	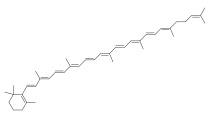	$[M+H]^+$	537.4372	537.4460	−16.37
10	Methyl gallate	$C_8H_8O_5$	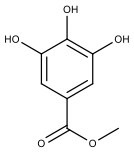	$[M+NH_4]^+$	202.0754	202.0715	19.30
11	Hesperidin	$C_{28}H_{34}O_{15}$	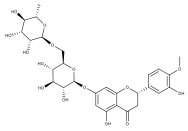	$[M+H]^+$	611.1968	611.1976	−1.31
12	Neohesperidin	$C_{28}H_{34}O_{15}$	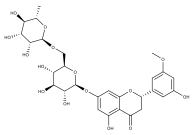	$[M+H]^+$	611.1968	611.1976	−1.31
13	Rutin	$C_{28}H_{34}O_{15}$	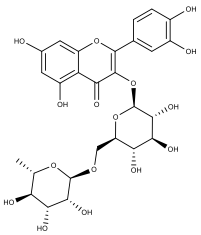	$[M+H]^+$	611.1968	611.1976	−1.31
14	Amygdalin	$C_{20}H_{27}NO_{11}$	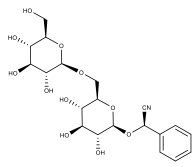	$[M+NH_4]^+$	475.1950	475.1928	4.63
15	Beta-Sitosterol	$C_{29}H_{50}O$	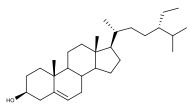	$[M+K]^+$	453.3460	453.3499	−8.60

(*Continued*)

Table 2 (Continued).

No.	Compounds	Formula	Chemical Structure	Ion Mode	Found Mass	Theo. MASS	Error/×10^{-6}
16	Ononin	$C_{22}H_{22}O_9$	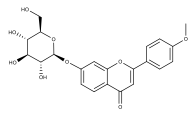	$[M+H]^+$	431.1372	431.1342	6.96
17	Alpha-Lactose	$C_{12}H_{22}O_{11}$	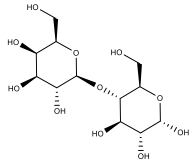	$[M+H]^+$	343.1279	343.1240	11.37
18	Poricoic acid AM	$C_{32}H_{48}O_5$	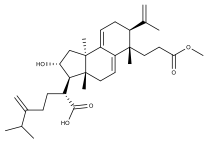	$[M+NH_4]^+$	530.3837	530.3845	−1.51
19	Poricoic acid D	$C_{31}H_{46}O_6$	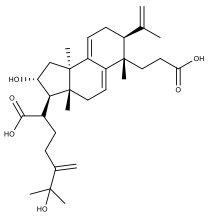	$[M+NH_4]^+$	532.3700	532.3638	11.65
20	Sucrose	$C_{12}H_{22}O_{11}$	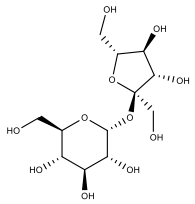	$[M+K]^+$	381.0817	381.0799	4.72

Effects of BSCO on Tumor Growth in Mice

Imaging results showed that fluorescence values in the model group were elevated and significantly higher than those in the BSCO-treated groups ($P < 0.05$, $P < 0.01$), suggesting that BSCO slowed the growth of LLC cells in mice. The positive control drug, cyclophosphamide, significantly inhibited the growth of LLC cells in mice compared with that in the model group ($P < 0.01$), as shown in Figure 2.

Histopathological Morphology Changes in the Lungs of Lewis Lung Cancer Mice

The results of H&E staining showed that lung tissue from mice in the model group had blurred cell edges, large and heterogeneous nuclei, and disturbed cell arrangement accompanied by partial alveolar rupture. Compared with the model group, lung tissue from the BSCO low-(0.2 mL/10 g), medium-(0.4 mL/10 g), and high-dose (0.8 mL/10 g) groups

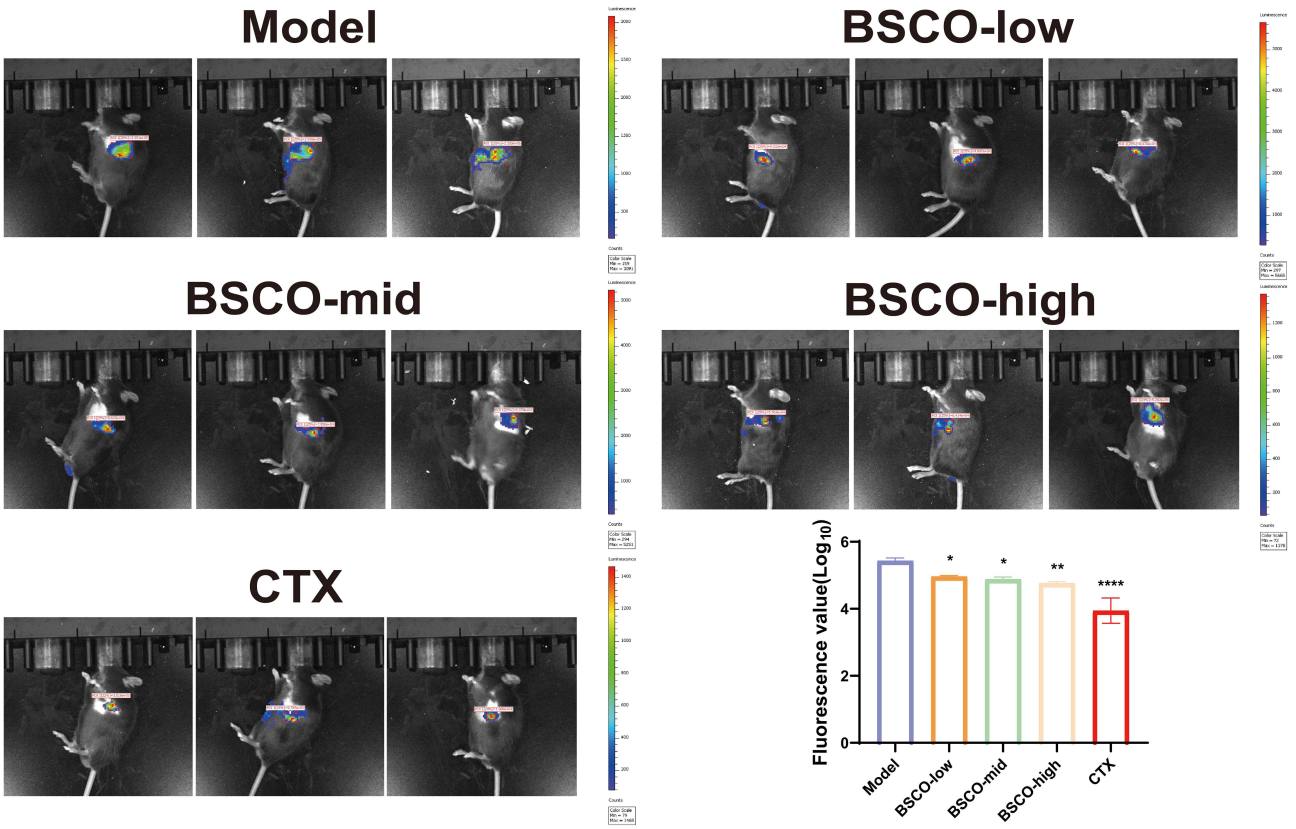

Figure 2 Effect of BSCO on tumors in lung cancer mice. Representative in-vivo fluorescence images for Model, BSCO-low/mid/high, and CTX; thoracic ROI fluorescence (log10) is quantified, and color bars show low-to-high signal. Data are shown as the mean ± SD; * $P < 0.05$, ** $P < 0.01$, **** $P < 0.0001$ vs the model group, n = 6.

showed varying degrees of cell necrosis accompanied by hemorrhage, and structural damage to the lung tissue was ameliorated. In the positive cyclophosphamide group (CTX), the cells were locally necrotic accompanied by mild hemorrhage, and a small number of necrotic cell fragments were seen, as shown in Figure 3.

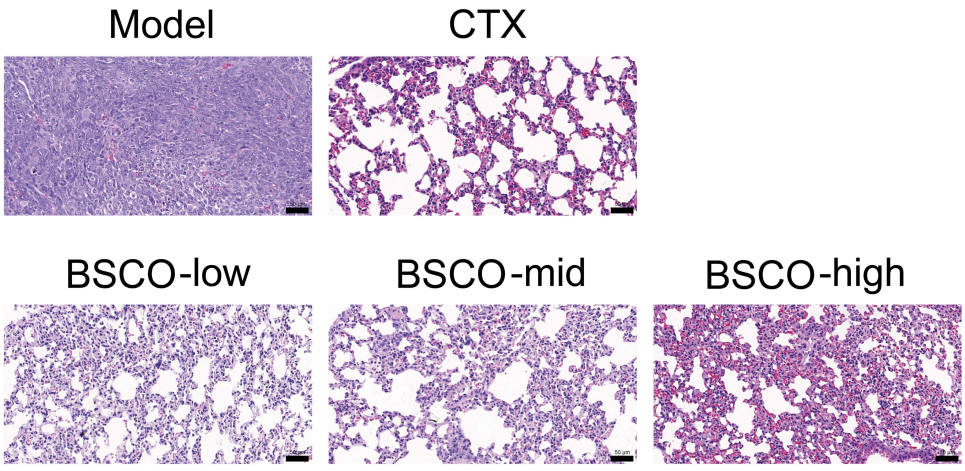

Figure 3 Effects of BSCO on histopathological morphology in the lungs of Lewis lung cancer mice (H&E, ×200). Representative hematoxylin–eosin–stained sections from Model, BSCO-low (0.2 mL/10 g), BSCO-mid (0.4 mL/10 g), BSCO-high (0.8 mL/10 g), and CTX (cyclophosphamide) groups.

Lung Cancer-Related Serum Indexes

Compared with the blank control group (Control), serum levels of CAT, GSH-Px, and SOD were significantly lower in the model mice (Model, $P < 0.001$), the detailed data are provided in Supplementary Table 1, while levels of PFK, GLUT1, HK2, MDA, and PK were significantly elevated ($P < 0.001$). These data indicated successful establishment of the model. Compared with the model group, treatment with BSCO increased the levels of CAT, GSH-Px, and SOD to varying degrees, and decreased the levels of PFK, GLUT1, HK2, MDA, and PK, with the high dose being the most effective ($P < 0.001$, Figure 4). The results suggest that BSCO has a certain ameliorative effect on Lewis lung cancer in mice.

Effect of BSCO and Drug-Containing Serum on Lung Cancer Cell Viability

BSCO at 100–200 mg/mL showed significant cytotoxicity towards Lewis cells at 24 h ($P < 0.05$), and the IC_{50} was calculated to be 173 mg/mL (Figure 5A and B). The 24 and 48 h data showed that low and high doses of BSCO as well as cyclophosphamide significantly inhibited the viability of Lewis cells compared to the blank group. Compared with the blank group, more apoptotic cells could be observed under the microscope after 72 hours of incubation with rat serum from the low-dose BSCO group, high-dose BSCO group, and cyclophosphamide group (Figure 5C).

Prediction of Targets and Pathways of BSCO in Lung Cancer Treatment via Network Pharmacology

A total of 17 active ingredients of BSCO were obtained using the SwissADME platform and relevant literature. These active ingredients were then searched in the Swiss Target Prediction, ETCM 2.0, and TCMSP databases to identify 460 therapeutic targets of BSCO. Additionally, by retrieving data from GeneCards, TTD, OMIM, and DisGeNET databases, a

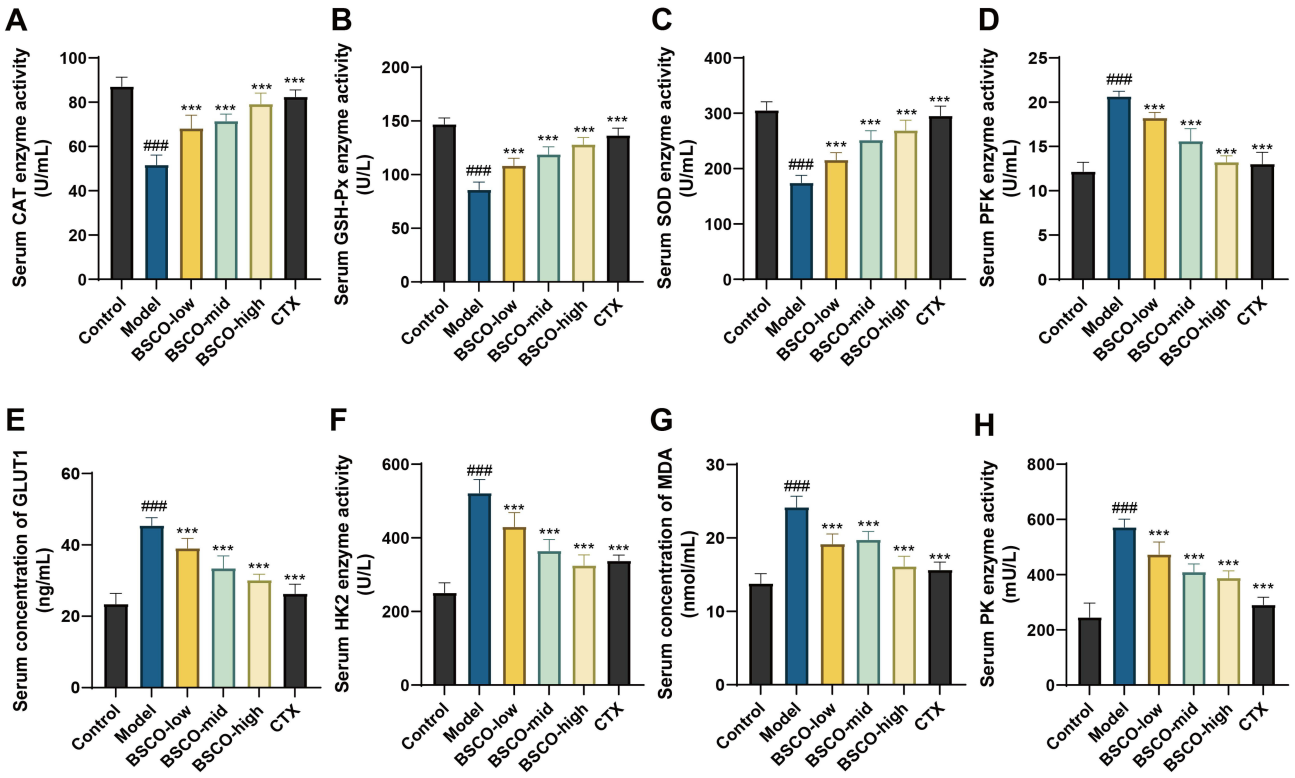

Figure 4 Effects of BSCO on serum indexes of Lewis lung cancer in mice. (**A**) CAT activity (U/mL); (**B**) GSH-Px activity (U/L); (**C**) SOD activity (U/mL); (**D**) PFK activity (U/mL); (**E**) GLUT1 concentration (ng/mL); (**F**) HK2 activity (U/L); (**G**) MDA concentration (nmol/mL); (**H**) PK activity (mU/L). Data are mean ± SD (n = 6). Statistics: ***P < 0.001 vs Model, ###P < 0.001 vs Control.

https://doi.org/10.2147/CMAR.S563551

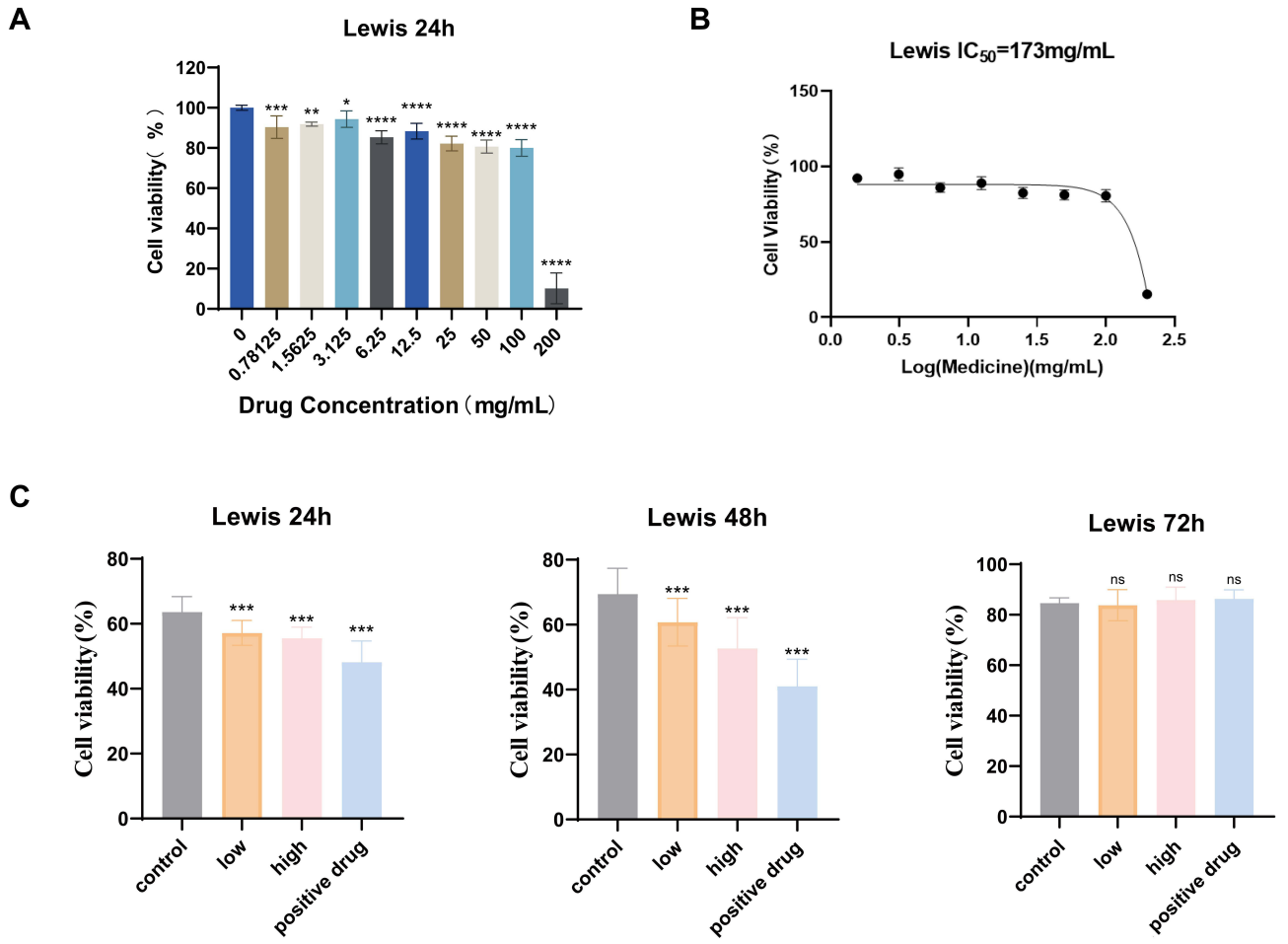

Figure 5 Effect of BSCO and drug-containing serum on Lewis cell viability. (**A**) 24 h dose–response of BSCO (0–200 mg/mL); viability normalized to control (100%). (**B**) IC_{50} determination by nonlinear fit of log_{10}[BSCO] versus viability (IC_{50} = 173 mg/mL). (**C**) Detection of cell viability using drug-containing serum at 24/48/72 h. Data are shown as the mean ± SD; * $P < 0.05$, ** $P < 0.01$, *** $P < 0.001$, **** $P < 0.0001$ vs the control group, ns indicates no significant difference n = 6.

total of 5184 lung cancer-related genes were identified, among which 341 genes overlapped with the BSCO therapeutic targets. A Venn diagram was created and is shown in Figure 6A.

The PPI network constructed from the STRING database consisted of 341 overlapping targets, including 341 nodes representing the targets and 6779 edges representing interactions. The data were imported into Cytoscape for analysis, where 51 hub genes were identified using topological parameter values. All nodes were ranked from high to low based on degree, with their sizes representing the degree and their colors ranging from dark to light. The results showed that the nodes representing GAPDH, AKT1, TP53, TNF and IL6 had larger areas and darker colors, indicating that these targets were of greater importance (Figure 6B).

Using the Metascape database, 3,572 GO terms were enriched when applying a filter of $P < 0.05$. Among these, 2,694 entries were related to biological processes (BP), including response to hormone, cellular response to nitrogen compound, and cellular response to hormone stimulus. The cellular component (CC) category contained 161 entries, particularly membrane raft, membrane microdomain, and neuronal cell body. The molecular function (MF) category included 327 entries, such as phosphotransferase activity, alcohol group as acceptor, kinase activity, and protein kinase activity. The top 10 entries in each category were analyzed and plotted (Figure 6C).

Similarly, KEGG enrichment analysis conducted using Metascape with a filter of $P < 0.05$ identified 230 pathways. Relevant information for the top 20 enriched pathways was imported through a bioinformatics platform to generate a

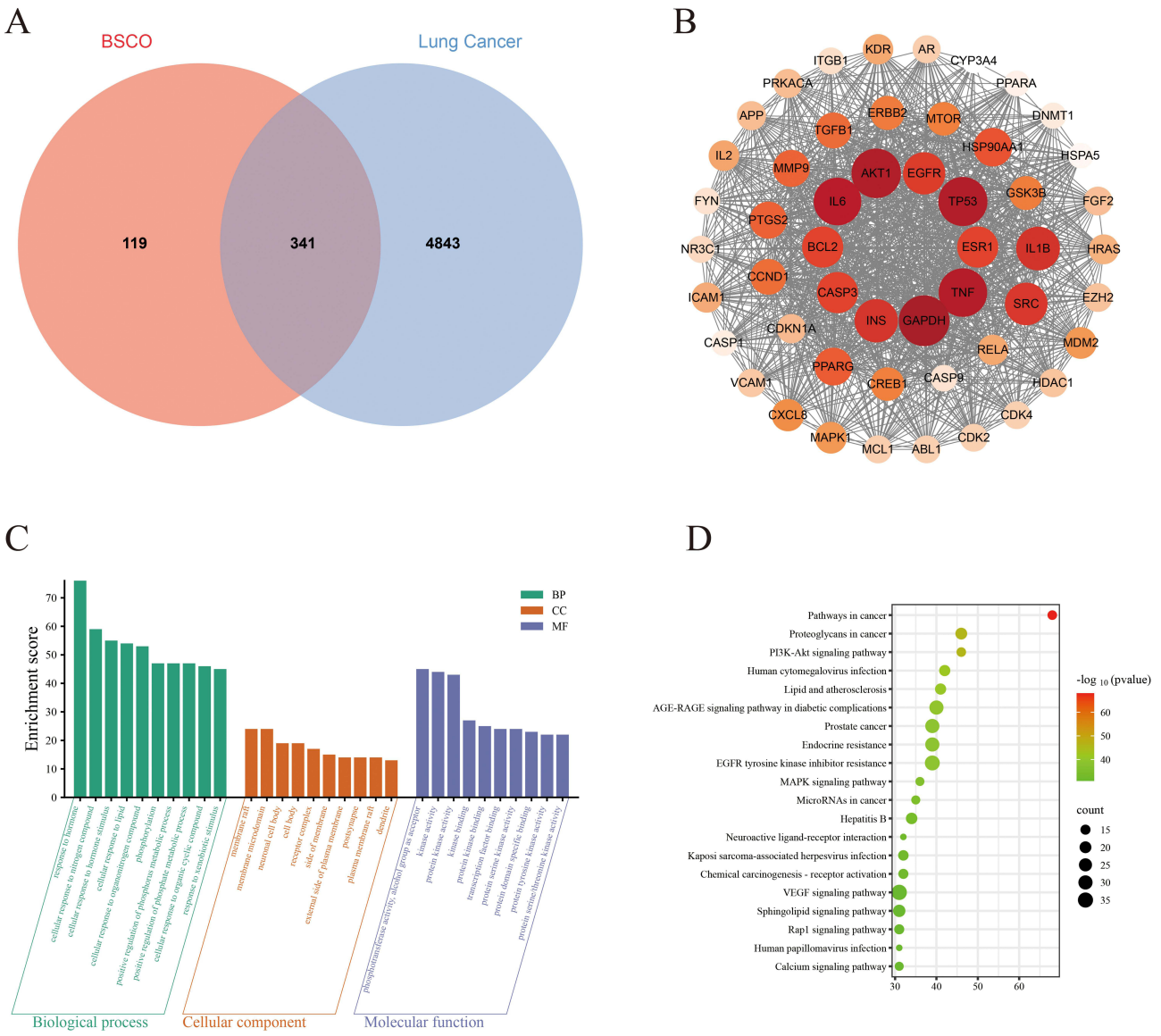

Figure 6 Network pharmacology analysis of BSCO in lung cancer. (**A**) Venn diagram of BSCO drug targets and lung cancer targets. (**B**) PPI network interaction diagram of BSCO and lung cancer shared hub targets. (**C**) GO enrichment analysis based on overlapping genes. (**D**) KEGG enrichment analysis based on overlapping genes.

KEGG enrichment pathway diagram. The results indicated that BSCO treatment of lung cancer primarily involves pathways such as Pathways in Cancer, Proteoglycans in Cancer, and the PI3K-Akt signaling pathway (Figure 6D).

Transcriptomic Analysis Reveals Differential Genes and Pathways

Principal component analysis showed clear separation between LC and BSCO groups (Figure 7A), supporting global transcriptomic shifts after BSCO treatment. To elucidate BSCO's therapeutic mechanisms in lung cancer, tumor tissues from BSCO-treated and untreated lung cancer mice underwent transcriptomic sequencing. Differentially expressed mRNAs ($|\log_2 FC| \geq 1.5$, FDR < 0.05) revealed 2,043 dysregulated genes (1,259 upregulated; 784 downregulated) (Figure 7B). Unsupervised hierarchical clustering (TreeView) visualized distinct intergroup expression patterns in a heatmap (Figure 7C).

Subsequently, KEGG pathway enrichment analysis was performed on the core targets that had been identified through transcriptomic approaches. This analysis revealed 239 enriched pathways, with the top 30 significantly enriched

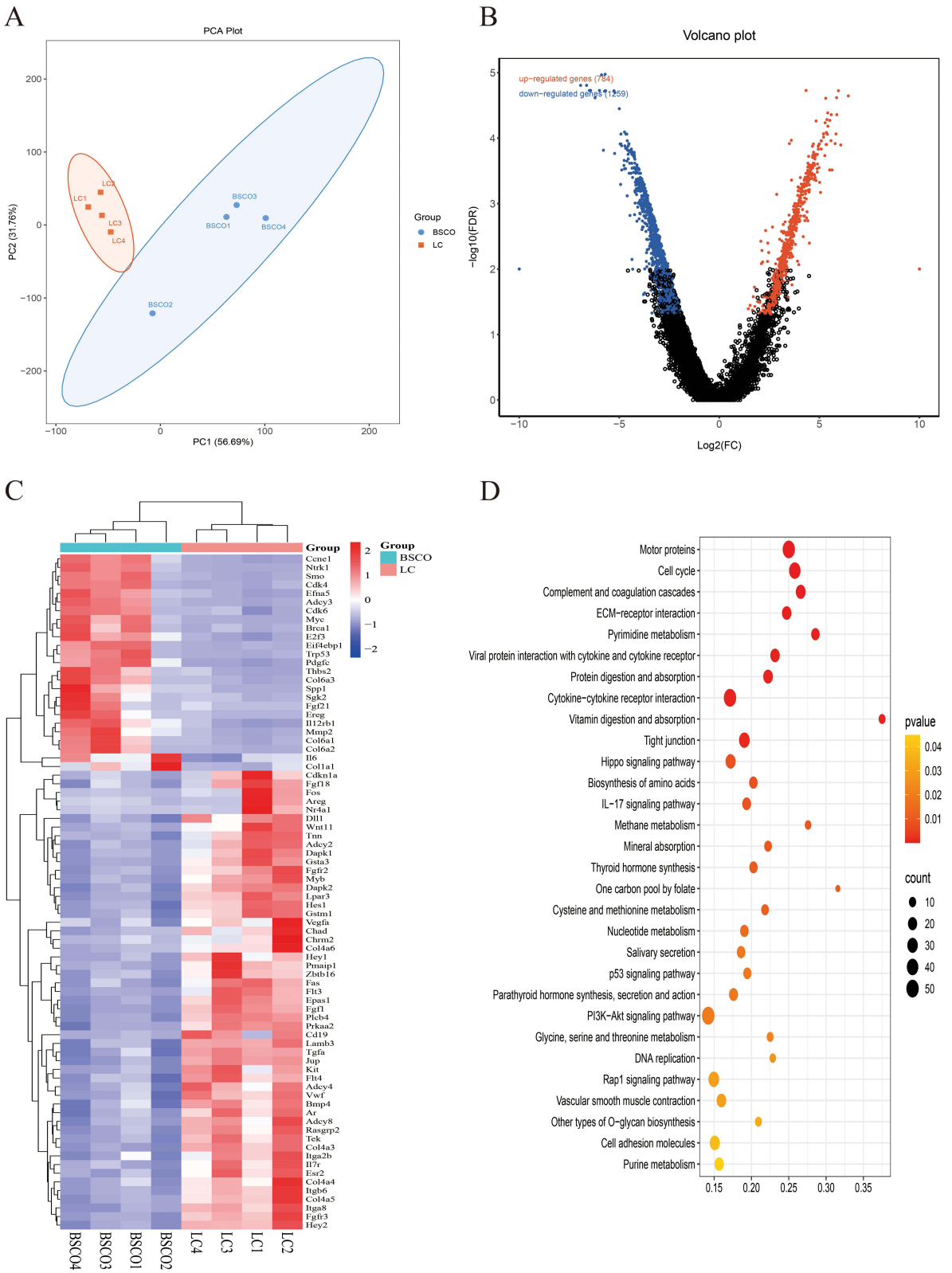

Figure 7 Transcriptomics analysis of BSCO treatment on tumor tissues of LC mice. (**A**) PCA plot of LC and BSCO. (**B**) DEGs volcano map of BSCO versus LC. (**C**) Hierarchical clustering heat maps of DEGs. (**D**) Bubble diagram of KEGG pathway enrichment of BSCO and LC common targets.

pathways visualized (see Figure 7D). When compared to the results of network pharmacology, both methods indicated notable alterations in the PI3K-Akt signaling pathway and the Rap1 signaling pathway.

Network Pharmacology Combined with Transcriptomics Exposed Key Molecules and Signaling Pathways Modulated by BSCO in Lung Cancer Mice

By integrating the results with network pharmacology, we intersected the differentially expressed genes with 341 therapeutic targets and identified 52 overlapping genes (Figure 8A), which are likely to constitute the key targets underlying BSCO's anti-lung cancer effects. Protein–protein interaction (PPI) analysis revealed a functional interaction network among these genes and identified several hub genes, including TP53, TNF, IL6, IL1B, and CASP3 (Figure 8B).

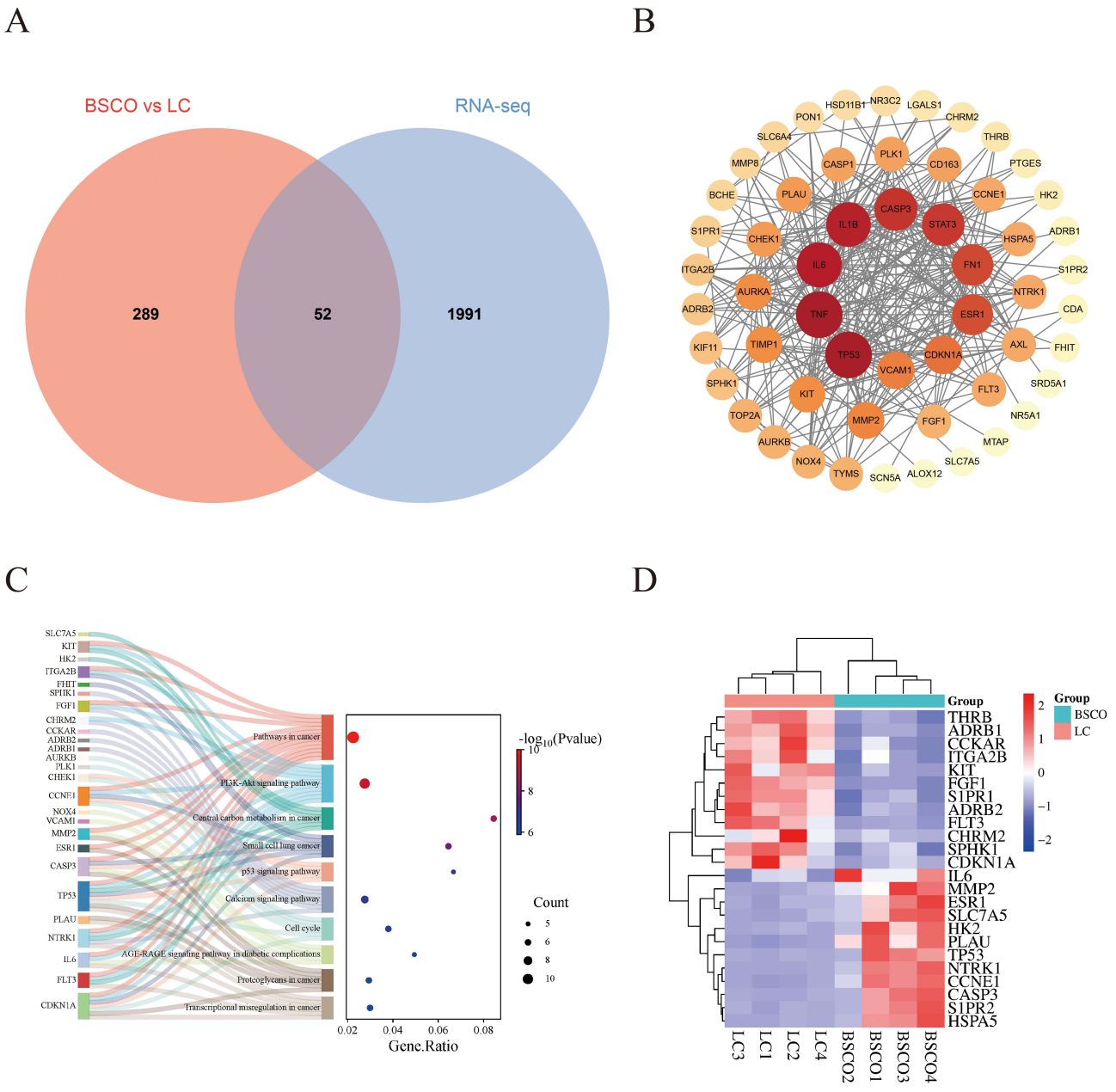

Figure 8 Integrated network pharmacology and transcriptomics analysis of tumor tissues from lung cancer mice treated with BSCO. (**A**) Venn diagram of genes identified from network pharmacology and RNA-seq differential expression analysis. (**B**) Protein–protein interaction (PPI) network of the overlapping genes. (**C**) Sankey Diagram of KEGG Enrichment for Key Genes. (**D**) Hierarchical clustering heatmap of key genes.

https://doi.org/10.2147/CMAR.S563551

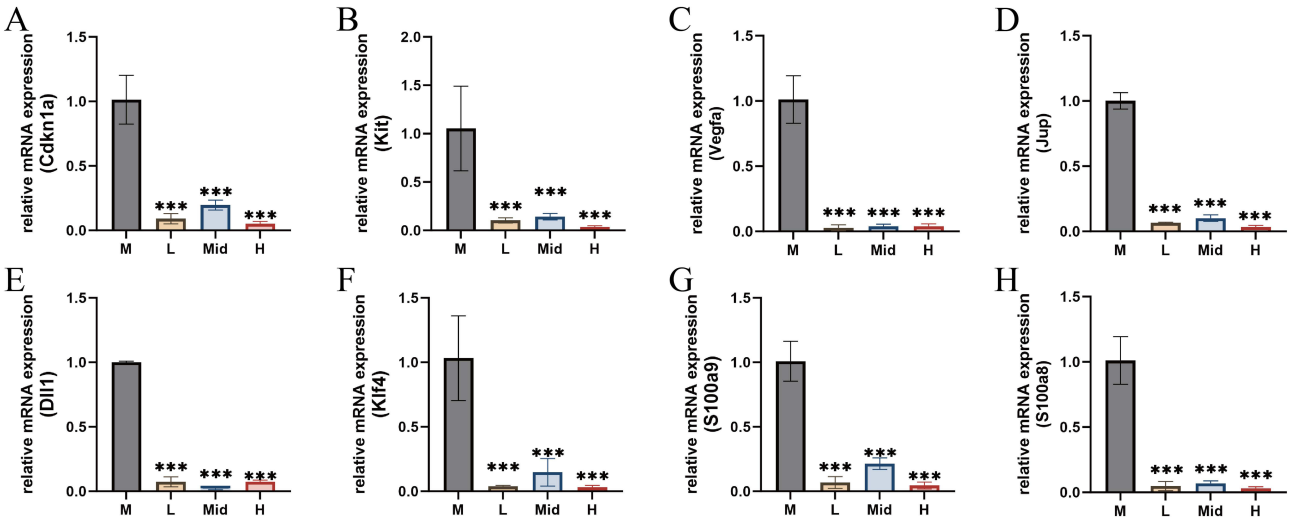

Figure 9 RT-qPCR validation of LC-related genes in tumor tissues after BSCO treatment. (**A**) CDKN1A; (**B**) KIT; (**C**) VEGFA; (**D**) JUP; (**E**) DLL1; (**F**) KLF4; (**G**) S100A8; (**H**) S100A9. (n = 3, data expressed as mean ± standard deviation ***P < 0.001 vs Model).

KEGG pathway enrichment analysis further associated these genes with the top 10 significantly enriched pathways (Figure 8C). The PI3K-Akt signaling pathway has once again been considered a key pathway, with genes such as TP53, IL6, CCNE1, CDKN1A, CHRM2, FGF1, FLT3, ITGA2B, KIT, and NTRK1 being notably enriched. According to the PPI network, TP53, IL6, CDKN1A and KIT are key genes in this pathway. Transcriptomic sequencing results of these critical targets are presented in Figure 8D.

To functionally validate the predictions from transcriptomic analysis, we quantitatively examined the mRNA expression of genes associated with lung cancer pathogenesis and those involved in the PI3K-Akt pathway. As critically demonstrated in Figure 9, administration of BSCO at test doses significantly modulated the expression of these targets compared with the model group ($p < 0.001$). Specifically, genes such as CDKN1A, KIT, VEGFA, JUP, DLL1, KLF4, S100A8, and S100A9 were significantly downregulated, consistent with the trends observed in the transcriptomic data, the reliability of the transcriptomics results has been verified.

Integrating evidence from both network pharmacology and transcriptome analyses, we propose that the PI3K-Akt signaling pathway may serve as a key regulatory axis through which BSCO exerts its anti-lung cancer effects, coordinating a tumor-suppressive response. This pathway has been shown to play a critical role in tumor cell proliferation, tumor microenvironment changes, angiogenesis, and tumor morphological alterations. Importantly, key genes within this pathway, including CDKN1A and KIT, were validated to be significantly downregulated. However, the exact mechanisms still need further validation.

Discussion

In recent years, an increasing number of traditional Chinese medicine and herbal therapies have been shown to be effective with few side effects, and traditional Chinese medicine is gradually aligning with modern medicine.[34] This research is based on the doctrine of constitution and medicinal paste, drawing on classic prescriptions and utilizing medicine food homology substances that meet safety requirements to create BSCO. BSCO has stronger safety compared to the original formula. Moreover, the potential efficacy of BSCO in treating lung cancer was confirmed through both in vitro and in vivo experiments. Subsequent integrated analysis using network pharmacology and transcriptomics identified potential therapeutic targets and pathways, further elucidating the underlying mechanisms of BSCO against lung cancer.

In this study, the histopathological morphology of mouse lung tissue was observed by H&E staining and showed that BSCO inhibited the growth of Lewis LC tumor cells in mice. This result was confirmed by fluorescence imaging of lung cancer mice. The efficacy of BSCO on lung cancer was evaluated from the cellular and serum pharmacological levels. BSCO was shown to inhibit proliferation of Lewis lung cancer cells with an IC50 of 173 mg/mL. The viability of Lewis

cells treated with serum from rats dosed with high and low doses of BSCO, and cyclophosphamide, was reduced after incubation for 24 and 48 h compared with the control. The effect of high dose BSCO serum was greater than that of low dose BSCO serum.

Our analysis suggested that the primary active component may be caffeic acid phenethyl ester (CAPE), a phenolic acid compound with potential as an anticancer agent. CAPE exerts its effects in cancer progression through the PI3K-Akt signaling pathways and adenosine monophosphate-activated protein kinase (AMPK) signaling pathways, which is consistent with predictions from network pharmacology and transcriptomics analysis KEGG analysis.[35,36]

Network pharmacology, transcriptomics and broader multi-omics are widely used to decode TCM formulas' multi-component mechanisms. In colorectal cancer, Li et al combined predicted herb–target networks with TCGA genes and RNA-seq, and validated that the FZXJJZ decoction suppresses metastasis via the VDR/TGF-β/Snail1 signaling pathways.[37] Complementing these, Huo et al used the same network pharmacology and transcriptomics workflow to pinpoint CYP24A1-mediated VDR and TERT-mediated Wnt pathways as actionable nodes for a *Ganoderma lucidum–Sanghuangporus vaninii* extract, corroborating anti-CRC effects in vitro and in vivo.[38] Combining network pharmacology and transcriptome analysis, the key targets include TP53, TNF, IL6, IL1B, and CASP3. TP53, TNF, IL1B, and CASP3 all play critical roles in cancer. TP53, a well-known tumor suppressor, primarily functions by inducing cell cycle arrest, senescence, or programmed apoptosis to prevent the proliferation of damaged cells. TNF, IL6, and IL1B are all immune-related molecules, with IL6 and IL1B key inflammatory cytokines closely associated with cancer progression. Many chemotherapeutic agents ultimately exert their anti-tumor effects by activating CASP3, which cleaves essential cellular substrates and leads to the orderly dismantling of the cell, thereby inducing apoptosis in cancer cells.[39] It is also speculated that BSCO may exert its anticancer effects through the PI3K-Akt signaling pathway. This pathway is crucial for cancer cell survival and affects tumor proliferation, apoptosis, and autophagy.[40] Importantly, as key genes in this pathway, TP53 and IL6 are significantly upregulated, while CDKN1A and KIT have been validated to be significantly downregulated. TP53 is a critical tumor suppressor gene. The inactivation of TP53 itself or its associated signaling pathways is a common feature in various human cancers. It plays a key role in regulating multiple biological processes, including DNA repair, cell cycle arrest, apoptosis, autophagy, cellular senescence, metabolism, and aging.[41,42] Furthermore, TP53 activates the transcription of CDKN1A, thereby mediating diverse biological functions. IL-6 generally promotes cancer progression by facilitating proliferation, invasion, metastasis, angiogenesis, and therapy resistance. However, its role in cancer is not exclusively detrimental, as it can also sensitize cells to TNF-α- and TRAIL/Apo2L-dependent cell death.[43] CDKN1A exhibits a dual role in tumor biology, it functions not only as a cell cycle inhibitor but also as a potential survival promoter under specific contexts, making its relationship with cancer outcomes complex.[44] KIT acts as a potent oncogenic driver by promoting uncontrolled cell proliferation and survival. Notably, BSCO effectively suppresses KIT expression, thereby inhibiting carcinogenesis.[45]

This study also verified the expression of some genes related to cancer. JUP is a key cell adhesion molecule involved in mediating cell-to-cell adhesion.[46] Studies demonstrate that HDAC7 drives lung cancer proliferation, migration, and invasion via JUP suppression, positioning the JUP axis as a promising therapeutic target.[47] VEGFA primarily promotes angiogenesis by binding to VEGFR2. This signaling cascade drives endothelial cell proliferation, migration, and survival, playing a crucial role in the tumor's ability to absorb nutrients and oxygen. Inhibiting VEGFA can effectively exert anti-tumor effects.[48] S100A8 and S100A9 play key roles in inflammation regulation and immune response. In lung cancer, S100 A8/9 is significantly upregulated in tumor tissues.[49] Furthermore, S100A8 has been shown to be involved in the PI3K-Akt pathway, thereby affecting tumor growth.[50] The above genes are all key genes in PI3K-Akt pathway, and their action on this pathway helps inhibit cancer.

The levels of SOD, GSH-Px, CAT, HK2, PFK, MDA, GLUT1, and PK serum markers were restored towards normal by BSCO in Lewis lung carcinoma mice, with the best effect seen at the high dose. BSCO regulates carbon metabolism and glucose uptake in cancer cells by affecting the PI3K-Akt signaling pathway. The PI3K-Akt signaling pathway is crucial in regulating cellular processes by activating downstream effectors, significantly contributing to tumor proliferation, invasion, and metastasis. One key aspect of AKT1 activation is its ability to enhance glucose uptake in cancer cells by modulating the expression of GLUT1.[51] Beyond enhancing glucose uptake, AKT1 regulates critical glycolytic enzymes—including HK2 and PFK—via both post-translational modifications and transcriptional control. This dual regulation ultimately drives PFK1 activation.[52] This was confirmed in subsequent experiments. The activation of both

PFK1 and GLUT1 facilitates cell proliferation and tumorigenesis.[53] As a result, targeting the PI3K-Akt pathway to control tumor metabolism has emerged as a potential therapeutic strategy for treating cancer.[54]

As an adjunct approach, BSCO is expected to synergize with evidence-based treatment regimens for non-small cell lung cancer in supportive care. Meta-analyses of Chinese herbal medicine (CHM) added to chemotherapy report improvements in quality of life and, in some datasets, response and survival, while CHM combined with EGFR-TKIs has shown longer progression-free survival versus TKIs alone.[55]

A major limitation of this study lies in its focus on the pharmacodynamic validation of BSCO both in vivo and in vitro, combined with preliminary gene and pathway predictions as well as mRNA verification via network pharmacology and transcriptomics. The absence of protein-level functional validation restricts the certainty regarding BSCO's mechanism in treating lung cancer. Nevertheless, further investigation into BSCO holds substantial promise. Based on these findings, future studies should focus on elucidating the precise mechanisms by which BSCO treats lung cancer, particularly its pharmacological effects on cell proliferation, inflammatory responses, and immunomodulatory mechanisms. Given its high half-maximal inhibitory concentration (IC50) and lack of protein-level validation, BSCO is likely to serve as an adjunct to guideline-directed therapy for non-small cell lung cancer (NSCLC), which still requires rigorous, interaction-conscious trials.

In summary, this study identified the chemical compounds contained in BSCO and experimentally validated these findings through both in vitro and in vivo approaches. Furthermore, network pharmacology and transcriptomics analyses were employed to predict the potential molecular targets, signaling pathways, and protein interactions regulated by these components. The results confirmed that BSCO exerts significant anti-cancer effects on lung cancer cells. BSCO has the potential to become an adjunct therapy in lung cancer treatment.

Conclusion

This study identified 20 major chemical components in BSCO. Both in vitro and in vivo experiments demonstrated that BSCO exhibits anti-lung cancer activity, effectively inhibiting cancer cell proliferation and tumor growth while restoring serum biochemical indicators associated with lung cancer. Preliminary analyses suggest that key targets of BSCO in the treatment of lung cancer include TP53, TNF, IL6, IL1B, and CASP3, indicating that its anti-cancer effects are likely mediated through the PI3K-Akt signaling pathway. Critical targets along this pathway, such as TP53, IL6, CDKN1A, and KIT were identified, the reliability of the transcriptomic results was confirmed by verifying some lung cancer-related genes through RT-qPCR. Upon completion of rigorous trials evaluating its safety and interactions, BSCO has the potential to become an adjunct therapy in lung cancer treatment.

Abbreviations

BSCO, Blood stasis constitution ointment; UPLC-Q-TOF-MS, Ultra-High Performance liquid chromatography electrospray ionization quadrupole time-of-flight mass spectrometry; LC, Lung cancer; MFH, Medicine-Food Homologous Substances; PPI, Protein-Protein Interaction; GO, Geneontology; KEGG, Kyoto encyclopedia of genes and genomes; BP, Biological Process; CC, Cellular Component; MF, Molecular Function; H&E, Hematoxylin-Eosin staining; PI3K-Akt, Phosphoinositide 3-Kinase/Protein Kinase B pathway; GAPDH, Glyceraldehyde-3-phosphate dehydrogenase; AKT1, Protein kinase B1; TP53, Tumor protein p53; TNF, Tumor Necrosis Factor; IL6, Interleukin 6; SOD, superoxide dismutase; GSH-Px, glutathione peroxidase; CAT, catalase; HK2, hexokinase 2; PFK, phosphofructokinase; MDA, malondialdehyde; GLUT1, glucose transporter protein 1; PK, pyruvate kinase; IL1B, Interleukin 1 Beta; CASP3, Caspase 3; CDKN1A, Cyclin Dependent Kinase Inhibitor 1A; KIT, Receptor Tyrosine Kinase; VEGFA, Vascular endothelial growth factor A; JUP, Junction plakoglobin; DLL1, Delta-like protein 1; S100A8, Calgranulin A; S100A9, Calgranulin B.

Ethics Statement (IRB Exemption)

This study used legally obtained public data and/or non-interventional observations of public behavior. All data were de-identified prior to analysis, with no direct interaction or intervention with human subjects, and no involvement of sensitive personal information or commercial interests. The study does not pose harm to humans. In accordance with Article 32 (1)–(2) of the Measures for Ethical Review of Life Science and Medical Research Involving Human Subjects (NHC et al, 2023), the study qualifies for exemption from IRB review.

Funding

This research was financially supported by National Intangible Cultural Heritage Project [IX-4(1)]; China Academy of Chinese Medical Sciences Science and Technology Innovation Project (CI2021A04313).

Disclosure

The authors declare no conflicts of interest.

The manuscript is also available on ResearchSquare (https://www.researchsquare.com/article/rs-5924974/v1), Preprint Title: Integrated UPLC-Q-TOF-MS, network pharmacology and experimental approach to evaluate the effects of blood stasis constitution ointment on lung cancer. DOI:https://doi.org/10.21203/rs.3.rs-5924974/v1

References

1. Lortet-Tieulent J, Renteria E, Sharp L, et al. Convergence of decreasing male and increasing female incidence rates in major tobacco-related cancers in Europe in 1988–2010. *Eur J Cancer*. 2015;51(9):1144–1163. doi:10.1016/j.ejca.2013.10.014
2. Sung H, Ferlay J, Siegel RL, et al. Global cancer statistics 2020: GLOBOCAN estimates of incidence and mortality worldwide for 36 cancers in 185 countries. *CA Cancer J Clin*. 2021;71(3):209–249. doi:10.3322/caac.21660
3. de Koning HJ, van der Aalst CM, de Jong PA, et al. Reduced lung-cancer mortality with volume CT screening in a randomized trial. *N Engl J Med*. 2020;382(6):503–513. doi:10.1056/NEJMoa1911793
4. Li R, Li J, Zhou X. Lung microbiome: new insights into the pathogenesis of respiratory diseases. *Signal Transduct Target Ther*. 2024;9:19. doi:10.1038/s41392-023-01722-y
5. Rammal S, Kourie HR, Jalkh N, et al. Molecular pathogenesis of hereditary lung cancer: a literature review. *Pharmacogenomics*. 2021;22(12):791–803. doi:10.2217/pgs-2020-0150
6. Zhang XX, Li ZG. Discussion on the etiology and pathogenesis of lung cancer in Traditional Chinese Medicine. *China Journal of Traditional Chinese Medicine and Pharmacy*. 2015;10:3447–3449.
7. Lemjabbar-Alaoui H, Hassan O, Yang YW, Buchanan P. Lung cancer: biology and treatment options. *Biochim Biophys Acta*. 2015;1856(2):189–210. doi:10.1016/j.bbcan.2015.08.002
8. O'Brien M, Paz-Ares L, Marreaud S, et al. Pembrolizumab versus placebo as adjuvant therapy for completely resected stage IB–IIIA non-small-cell lung cancer (PEARLS/KEYNOTE-091): an interim analysis of a randomised, triple-blind, Phase 3 trial. *Lancet Oncol*. 2022;23(10):1274–1286. doi:10.1016/S1470-2045(22)00518-6
9. Tsuboi M, Herbst RS, John T, et al. Overall survival with osimertinib in resected mutated NSCLC. *N Engl J Med*. 2023;389(2):137–147. doi:10.1056/NEJMoa2304594
10. Li C-L, Hsia T-C, Li C-H, Chen K-J, Yang Y-H, Yang S-T. Adjunctive traditional Chinese medicine improves survival in patients with advanced lung adenocarcinoma treated with first-line epidermal growth factor receptor (EGFR) tyrosine kinase inhibitors (TKIs): a nationwide, population-based cohort study. *Integr Cancer Ther*. 2019;18:1534735419827079. doi:10.1177/1534735419827079
11. Li J, Zhu GH, Liu TT, Xu BW, Li J. Comparative efficacy of 10 Chinese herbal injections combined with GP regimen chemotherapy for patients with advanced NSCLC a systematic review and network meta-analysis. *J Cancer*. 2022;13(2):465–480. doi:10.7150/jca.66410
12. Wong W, Lam CLK, Wong VT, Yang ZM, Ziea ETC, Kwan AKL. Validation of the constitution in Chinese medicine questionnaire: does the traditional chinese medicine concept of body constitution exist? *Evid Based Complement Alternat Med*. 2013;2013:481491. doi:10.1155/2013/481491
13. Cho W, Kim JH, Jeong M, et al. Pattern identification of lung cancer patients based on body constitution questionnaires (BCQ) and glycoproteomics for precision medicine. *Medicine*. 2019;98(24):e16035. doi:10.1097/MD.0000000000016035
14. Han ZQ, Deng DH, Feng YH, et al. Study on correlation between polymorphism of CHRNB4 rs7178270 and blood stasis patients with lung cancer. *Chinese Archives of Traditional Chinese Medicine*. 2020;38:90–93. doi:10.13193/j.issn.1673-7717.2020.06.022
15. Bi JF, Zhang H. Observation of therapeutic effects of Buyang Huanwu Decoction combined with moxibustion in the treatment of elderly patients with advanced lung cancer. *Beijing J TCM*. 2023;03:338–342. doi:10.16370/j.cnki.13-1214/r.2024.03.005
16. Nian H, Zhang QQ, Ma MH, et al. Clinical application of gaofang (medicated paste) in cardiovascular disease. *Chin Med Culture*. 2022;5(3):190–197. doi:10.1097/MC9.0000000000000029
17. Wang X, Xing X, Huang P, et al. A Chinese classical prescription Xuefu Zhuyu decoction in the treatment of coronary heart disease: an overview. *Heliyon*. 2024;10(7):e28919. doi:10.1016/j.heliyon.2024.e28919
18. Xu Y, Chen B, Yi J, et al. Buyang Huanwu decoction alleviates cerebral ischemic injury through modulating caveolin-1-mediated mitochondrial quality control. *Front Pharmacol*. 2023;14:1137609. doi:10.3389/fphar.2023.1137609
19. Feng Y, Dai L, Zhang Y, et al. Buyang Huanwu decoction alleviates blood stasis, platelet activation, and inflammation and regulates the HMGB1/NF-κB pathway in rats with pulmonary fibrosis. *J Ethnopharmacol*. 2024;319:117088. doi:10.1016/j.jep.2023.117088
20. Li H, Zhang W, Lou Q, Chang Y, Lin Z, Lou L. XueFu ZhuYu decoction alleviates cardiopulmonary bypass-induced nlrp3 inflammasome-dependent pyroptosis by inhibiting IkB-α/NF-κB pathway in acute lung injury rats. *Evid Based Complement Alternat Med*. 2022;2022:1–15. doi:10.1155/2022/6248870
21. Hammes M. Huang di nei jing su wen – an annotated translation of huang di's inner classic – basic questions. *Deutsche Zeitschrift für Akupunktur*. 2013;56(2):55. doi:10.1016/j.dza.2013.06.025
22. You L, Cha S, Kim MY, Cho JY. Ginsenosides are active ingredients in panax ginseng with immunomodulatory properties from cellular to organismal levels. *J Ginseng Res*. 2022;46(6):711–721. doi:10.1016/j.jgr.2021.12.007
23. Zhang L, Xu Z, Jiang T, et al. Efficacy and safety of ejiao (asini corii colla) in women with blood deficient symptoms: a randomized, double-blind, and placebo-controlled clinical trial. *Front Pharmacol*. 2021;12:718154. doi:10.3389/fphar.2021.718154

24. Huang TY, Yang FL, Chiu HW, et al. An immunological polysaccharide from tremella fuciformis: essential role of acetylation in immunomodulation. *IJMS*. 2022;23(18):10392. doi:10.3390/ijms231810392
25. Feng L, Xiao X, Liu J, et al. Immunomodulatory effects of lycium barbarum polysaccharide extract and its uptake behaviors at the cellular level. *Molecules*. 2020;25(6):1351. doi:10.3390/molecules25061351
26. Wu M, Liu L, Xing Y, Yang S, Li H, Cao Y. Roles and mechanisms of hawthorn and its extracts on atherosclerosis: a review. *Front Pharmacol*. 2020;11:118. doi:10.3389/fphar.2020.00118
27. Gourineni V, Stewart M, Icoz D, Zimmer J. Gastrointestinal tolerance and glycemic response of isomaltooligosaccharides in healthy adults. *Nutrients*. 2018;10(3):301. doi:10.3390/nu10030301
28. Meunier M, Schinkovitz A, Derbré S. Current and emerging tools and strategies for the identification of bioactive natural products in complex mixtures. *Nat Prod Rep*. 2024;41(11):1766–1786. doi:10.1039/D4NP00006D
29. Xu L, Liu Y, Wu H, Wu H, Liu X, Zhou A. Rapid identification of chemical profile in gandou decoction by UPLC-Q-TOF-MSE coupled with novel informatics UNIFI platform. *J Pharm Anal*. 2020;10(1):35–48. doi:10.1016/j.jpha.2019.05.003
30. Liu P, Zhao L, Senovilla L, Kepp O, Kroemer G. In vivo imaging of orthotopic lung cancer models in mice. *Methods Mol Biol*. 2021;2279:199–212. doi:10.1007/978-1-0716-1278-1_16
31. Ibrahim AH, Khan MSS, Al-Rawi SS, et al. Safety assessment of widely used fermented virgin coconut oil (cocos nucifera) in Malaysia: chronic toxicity studies and SAR analysis of the active components. *Regul Toxicol Pharm*. 2016;81:457–467. doi:10.1016/j.yrtph.2016.10.004
32. Hanif A, Ibrahim AH, Ismail S, et al. Cytotoxicity against A549 human lung cancer cell line via the mitochondrial membrane potential and nuclear condensation effects of nepeta paulsenii briq. a perennial herb. *Molecules*. 2023;28(6):2812. doi:10.3390/molecules28062812
33. Ge J, Wang D, He R, Zhu H, Wang Y, He S. Medicinal herb research: serum pharmacological method and plasma pharmacological method. *Biol Pharm Bull*. 2010;33(9):1459–1465. doi:10.1248/bpb.33.1459
34. Peng L, Zhang K, Li Y, Chen L, Gao H, Chen H. Real-world evidence of traditional Chinese medicine (TCM) treatment on cancer: a literature-based review. *Evid Based Complement Alternat Med*. 2022;2022:1–10. doi:10.1155/2022/7770380
35. Elumalai P, Muninathan N, Megalatha ST, et al. An insight into anticancer effect of propolis and its constituents: a review of molecular mechanisms. *Evid Based Complement Alternat Med*. 2022;2022:1–14. doi:10.1155/2022/5901191
36. Mirzaei S, Gholami MH, Zabolian A, et al. Caffeic acid and its derivatives as potential modulators of oncogenic molecular pathways: new hope in the fight against cancer. *Pharmacol Res*. 2021;171:105759. doi:10.1016/j.phrs.2021.105759
37. Li Q, Chen JX, Wu Y, et al. The mechanism of FZXJJZ decoction suppresses colorectal liver metastasis via the VDR/TGF-β/Snail1 signaling pathways based on network pharmacology-TCGA data-transcriptomics analysis. *J Ethnopharmacol*. 2022;287:114904. doi:10.1016/j.jep.2021.114904
38. Huo J, Nie K, Yang T, et al. Network pharmacology combined with transcriptomics reveals that ganoderma lucidum spore and sanghuangporus vaninii compound extract exerts anti-colorectal cancer effects via CYP24A1-mediated VDR pathway and TERT-mediated wnt signaling pathway. *J Ethnopharmacol*. 2025;348:119820. doi:10.1016/j.jep.2025.119820
39. Soung Y, Lee J, Kim S, et al. Somatic mutations of CASP3 gene in human cancers. *Hum Genet*. 2004;115(2). doi:10.1007/s00439-004-1129-3
40. Huang R, Dai Q, Yang R, et al. A review: PI3K/AKT/mTOR signaling pathway and its regulated eukaryotic translation initiation factors may be a potential therapeutic target in esophageal squamous cell carcinoma. *Front Oncol*. 2022;12:817916. doi:10.3389/fonc.2022.817916
41. Donehower LA, Soussi T, Korkut A, et al. Integrated analysis of TP53 gene and pathway alterations in the cancer genome atlas. *Cell Rep*. 2019;28(5):1370–1384.e5. doi:10.1016/j.celrep.2019.07.001
42. Mogi A, Kuwano H. TP53 mutations in nonsmall cell lung cancer. *Biomed Res Int*. 2011;2011(1):583929. doi:10.1155/2011/583929
43. Huynh J, Ernst M. IL6 signaling in cancer: not always bad news. *Cancer Res*. 2021;81(18):4671–4672. doi:10.1158/0008-5472.CAN-21-2137
44. Manousakis E, Miralles CM, Esquerda MG, Wright RHG. CDKN1A/p21 in breast cancer: part of the problem, or part of the solution? *Int J Mol Sci*. 2023;24(24):17488. doi:10.3390/ijms242417488
45. Ashman LK, Griffith R. Therapeutic targeting of c-KIT in cancer. *Expert Opin Invest Drugs*. 2013;22(1):103–115. doi:10.1517/13543784.2013.740010
46. Ding W, Sun J, Song S, et al. Junction plakoglobin – a dual-role player in cancer biology. *Int J Surg*. 2025;111(6):3920–3930. doi:10.1097/JS9.0000000000002365
47. Sang Y, Sun L, Wu Y, Yuan W, Liu Y, Li SW. Histone deacetylase 7 inhibits plakoglobin expression to promote lung cancer cell growth and metastasis. *Int J Oncol*. 2019;54(3):1112–1122. doi:10.3892/ijo.2019.4682
48. Lin S, Hong M, Zhang J, et al. Characterization and functional evaluation of JS207, a novel bispecific antibody against human PD-1 and VEGFA. *Front Immunol*. 2025;16:1612547. doi:10.3389/fimmu.2025.1612547
49. Wang T, Liu R. S100 protein family in lung cancer: an updated narrative review. *CMAR*. 2025;17:713–722. doi:10.2147/CMAR.S508047
50. Ma X, Wu Y, Cao G. S100A8 mediates autophagy and apoptosis in ovarian cancer cells via the PI3K/akt pathway. *Discov Med*. 2025;37(197):1117. doi:10.24976/Discov.Med.202537197.99
51. Hosios AM, Manning BD. Cancer signaling drives cancer metabolism: AKT and the warburg effect. *Cancer Res*. 2021;81(19):4896–4898. doi:10.1158/0008-5472.CAN-21-2647
52. Hoxhaj G, Manning BD. The PI3K–AKT network at the interface of oncogenic signalling and cancer metabolism. *Nat Rev Cancer*. 2020;20(2):74–88. doi:10.1038/s41568-019-0216-7
53. Lee JH, Liu R, Li J, et al. EGFR-phosphorylated platelet isoform of phosphofructokinase 1 promotes PI3K activation. *Molecular Cell*. 2018;70(2):197–210.e7. doi:10.1016/j.molcel.2018.03.018
54. Zhang W, Cai S, Qin L, et al. Alkaloids of aconiti lateralis radix praeparata inhibit growth of non-small cell lung cancer by regulating PI3K/akt-mTOR signaling and glycolysis. *Commun Biol*. 2024;7(1):1118. doi:10.1038/s42003-024-06801-6
55. Wang LC, Chang YY, Lee IC, Kuo HC, Tsai MY. Systematic review and meta-analysis of Chinese herbal medicine as adjuvant treatment in advanced non-small cell lung cancer patients. *Complement Ther Med*. 2020;52:102472. doi:10.1016/j.ctim.2020.102472